Inverse Problems **16** (2000) 469–482. Printed in the UK PII: S0266-5611(00)04847-4

Imaging the solidification of molten metal by eddy currents: I

Minh H Pham†, Yingbo Hua† and Neil B Gray‡

† The Department of Electrical and Electronic Engineering, The University of Melbourne, Parkville, Victoria 3052, Australia
‡ G K Williams Co-operative Research Centre for Extractive Metallurgy, Department of Chemical Engineering, The University of Melbourne, Parkville, Victoria 3052, Australia

E-mail: minhpham@ee.mu.oz.au and yhua@ee.mu.oz.au

Received 27 May 1999, in final form 20 December 1999

Abstract. This paper presents an eddy-current-based technique for imaging the solidification of molten metal inside a metal pipe. This technique is motivated by the fact that the ac (alternating current) impedance seen from a solenoid placed outside the pipe is dependent on the distribution of the solidification inside the pipe provided that the ac frequency is properly chosen and the overall thickness of the pipe and solidification is small. This paper first establishes a simplified mathematical model based on the fundamental electromagnetic theory, which reveals the exact relationship between the solidification inside the pipe and the scattered field outside the pipe. Based on this model, an iterative algorithm for reconstructing the solidification distribution is then developed.

(Some figures in this article appear in colour in the electronic version; see www.iop.org)

1. Introduction

A molten metal flow electronic control system has been desired for a long time in the metallurgical field [1]. An essential part of such a system is a device that can image molten metal solidification inside a pipe. Since the conductivity of molten metal differs from that of solidification, the distribution of the solidification is readily revealed by a conductivity distribution. Due to the high conductivity of metals and the high temperature associated with molten metals, the resistance measurements on the (metal) pipe would be highly corrupted by noise and hence a conventional electrical resistance tomography technique such as that given in [2] is not applicable.

There appears to be no approach applicable for this imaging task other than that of eddy currents. The eddy-current technique is a nondestructive technique for determining the conductivity of metals [3, 4]. It employs low-frequency magnetic fields which penetrate into metals and create the so-called eddy currents. Eddy currents have a reasonable sensitivity to continuous and discontinuous changes in metals. Applications of eddy currents in the casting of molten metal can be found in [5, 6] and the more recent work [7]. To our knowledge, applying eddy currents for imaging metal solidification has not been reported before in the literature, except in the one-dimensional case [5].

0266-5611/00/020469+14$30.00

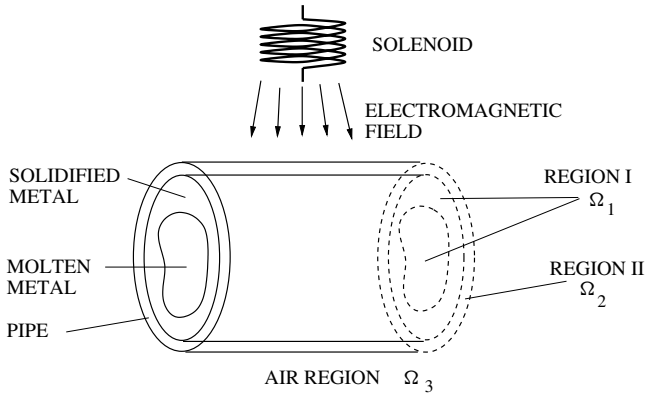

Figure 1. The problem geometry.

2. Description of the problem

The geometry of the problem is shown in figure 1. There are two types of media considered here, namely air and conductor. The cylindrical pipe containing molten metal is penetrated with a time-varying magnetic field from a solenoid. This field creates eddy currents circulating in the conductor. The pattern of the current depends on the conductivity distribution. The eddy currents in turn produce a scattered field which can be sensed in the region exterior to the pipe. Based on the external measurements, the shape and thickness of the solidification can be determined.

We will assume that the cylindrical pipe under consideration is penetrated with a transverse magnetic (TM) field. This TM field can be generated by a long rectangular solenoid where the end effect is neglected. Since the solidification is assumed to be invariant in the z direction, the dominating field is approximately z invariant. The problem is hence reduced to a two-dimensional one. The TM field consists of two components: an angular component and a radial component. In this paper, the materials are assumed to be linear and nonferromagnetic. For simplicity, relative permeability and permittivity are assumed to be unity. For low-frequency applications, displacement currents are negligible.

3. Modelling

3.1. Conductivity profile modelling

The geometry of the boundary between the solid and the melt is denoted by $\rho(\phi)$, $0 \leqslant \phi \leqslant 2\pi$. In general, there is also a 'mushy' zone, where the solid and liquid phases co-exist. Microscopic investigation of this zone has been carried out by many researchers [8, 9]. We, however, only consider the macroscopic property of the mushy region by assuming that the conductivity is smoothly distributed as shown in figure 2.

The conductivity distribution $\sigma_1(\boldsymbol{r})$ is modelled as follows:

$$\sigma_1(\boldsymbol{r}) = \sigma_s \left\{ 1 - \frac{\sigma_s - \sigma_l}{\sigma_s} f(\boldsymbol{r}) \right\} \tag{1}$$

where σ_s is the conductivity of the solidified metal; σ_l is the conductivity of molten metal;

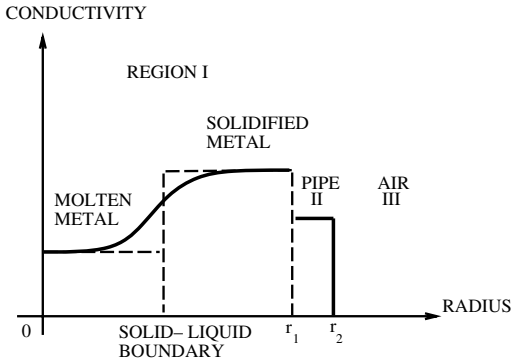

Figure 2. Conductivity profile.

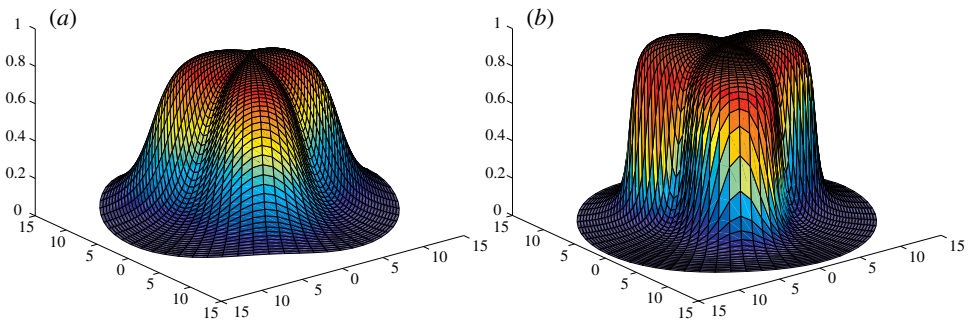

Figure 3. Examples of conductivity distribution where $\rho(\phi) = 10 + 2\sin(3\phi)$ and (*a*) $\alpha = 0.5$, (*b*) $\alpha = 2.0$.

$f(\boldsymbol{r})$ is defined as

$$f(\boldsymbol{r}) = \frac{1}{2} - \frac{\tan^{-1}\{\alpha[r - \rho(\phi)]\}}{\pi} \tag{2}$$

which is a monotonic function of r. The parameter α determines the thickness of the mushy zone between the solid and the liquid. Figure 3 shows two examples of $f(\boldsymbol{r})$. It should be kept in mind that $f(\boldsymbol{r})$ depends on the shape function $\rho(\phi)$ and the parameter α. Since the conductivity distribution $\sigma_1(\boldsymbol{r})$ is proportional to $f(\boldsymbol{r})$, we will refer to each of them as the distribution or profile. Note that as α approaches ∞, the mushy zone disappears since f approaches a step function:

$$f(\boldsymbol{r}) = \begin{cases} 1 & \text{if} \quad r < \rho(\phi) \\ 0 & \text{if} \quad r > \rho(\phi) \end{cases} \qquad 0 < \rho(\phi) < r_1 \tag{3}$$

where r_1 is the radius of region I.

In region I (Ω_1), the conductivity varies continuously. Region II (Ω_2) is the pipe and region III (Ω_3) is the air region outside the pipe which has zero conductivity.

3.2. Basic differential equations of our problem

The electric field (and hence eddy-current) distribution inside the pipe is described by quasi-static Maxwell's equations [10]. The diffusion equation for the time harmonic electric field

E_1 is given by

$$\begin{aligned} &\nabla^2 E_1(\boldsymbol{r}) - k_1^2 E_1(\boldsymbol{r}) = -\kappa f(\boldsymbol{r}) E_1(\boldsymbol{r}), \qquad k_1^2 = \mathrm{j}\omega\mu\sigma_s, \\ &\kappa = k_1^2 \frac{\sigma_s - \sigma_l}{\sigma_s}, \qquad \boldsymbol{r} \in \Omega_1 \end{aligned} \tag{4}$$

where $\mathrm{j} = \sqrt{-1}$, and ω is the frequency of the field. The term on the right-hand side of equation (4) represents the change of eddy-current distribution with respect to the background conductivity σ_s. The electric fields in the remaining regions II (pipe) and III (air) are

$$\nabla^2 E_2(\boldsymbol{r}) - k_2^2 E_2(\boldsymbol{r}) = 0, \qquad k_2^2 = \mathrm{j}\omega\mu\sigma_2, \quad \boldsymbol{r} \in \Omega_2 \tag{5}$$

$$\nabla^2 E_3(\boldsymbol{r}) - k_3^2 E_3(\boldsymbol{r}) = \mathrm{j}\omega\mu J(\boldsymbol{r}) \qquad k_3^2 = -\omega^2\mu\epsilon, \quad \boldsymbol{r} \in \Omega_3 \tag{6}$$

where σ_2 is the conductivity of the pipe, and $J(\boldsymbol{r})$ the current source in the air region. Since the frequency ω under consideration is relatively small, k_3 is negligible. Equations (4)–(6) together with appropriate boundary conditions completely describe the behaviour of the electromagnetic field in our setting. In the context of this paper, the boundary conditions require the field and its normal derivative to be continuous at the interfaces.

4. The relationship between the conductivity profile and the scattered field

Considering (4)–(6), we define the Green function G_u^v for region u due to the source in region v such that it satisfies the following:

$$\nabla^2 G_u^v(\boldsymbol{r}, \boldsymbol{r}') - k_u^2 G_u^v(\boldsymbol{r}, \boldsymbol{r}') = -\delta(\boldsymbol{r} - \boldsymbol{r}'), \qquad \boldsymbol{r} \in \Omega_u, \quad \boldsymbol{r}' \in \Omega_v. \tag{7}$$

It is assumed that G_u^v and its normal derivative are also continuous at the interfaces. It follows from the superposition theorem that

$$E_1(\boldsymbol{r}) = -\mathrm{j}\omega\mu \int_{\Omega_3} G_1^3(\boldsymbol{r}, \boldsymbol{r}') J(\boldsymbol{r}')\, \mathrm{d}\Omega' + \kappa \int_{\Omega_1} G_1^1(\boldsymbol{r}, \boldsymbol{r}') f(\boldsymbol{r}') E_1(\boldsymbol{r}')\, \mathrm{d}\Omega' \tag{8}$$

$$E_3(\boldsymbol{r}) = -\mathrm{j}\omega\mu \int_{\Omega_3} G_3^3(\boldsymbol{r}, \boldsymbol{r}') J(\boldsymbol{r}')\, \mathrm{d}\Omega' + \kappa \int_{\Omega_1} G_3^1(\boldsymbol{r}, \boldsymbol{r}') f(\boldsymbol{r}') E_1(\boldsymbol{r}')\, \mathrm{d}\Omega'. \tag{9}$$

The electric field $E_2(\boldsymbol{r})$ in region II is of no interest to us. In the literature (8) is standardly known as the domain equation and (9) as the data equation. The first integral in each of (8) and (9) represents the contribution from the applied current source. Therefore, the incident field is given by

$$E_{iu}(\boldsymbol{r}) = -\mathrm{j}\omega\mu \int_{\Omega_3} G_u^3(\boldsymbol{r}, \boldsymbol{r}') J(\boldsymbol{r}')\, \mathrm{d}\Omega', \qquad u = 1, 3. \tag{10}$$

The observable scattered field is defined as

$$E_s(\boldsymbol{r}) = E_3(\boldsymbol{r}) - E_{i3}(\boldsymbol{r}) = \kappa \int_{\Omega_1} G_3^1(\boldsymbol{r}, \boldsymbol{r}') f(\boldsymbol{r}') E_1(\boldsymbol{r}')\, \mathrm{d}\Omega'. \tag{11}$$

Equations (8) and (11) define the relationship between the distribution $f(\boldsymbol{r})$ and the observable scattered field $E_s(\boldsymbol{r})$. The Green functions are independent of $f(\boldsymbol{r})$ and hence can be computed off-line. The appendix shows the analytical expression of the Green functions.

5. Solution of the electric field by the moments method

The electric field $E_1(\boldsymbol{r})$ governed by (8) can be solved using the moments method [11, 12] with a proper choice of basis functions [13]. A natural choice of the basis functions is shown in the following series expansion:

$$E_1(\boldsymbol{r}) = \sum_{p=0}^{P} \sum_{q=0}^{Q} a_{pq} \cos(p\phi) r^q + \sum_{p=1}^{P} \sum_{q=0}^{Q} b_{pq} \sin(p\phi) r^q \tag{12}$$

where a_{pq} and b_{pq} are unknown complex coefficients. However, for large p the basis functions $\cos(p\phi)$ and $\sin(p\phi)$ oscillate rapidly, making numerical integration more difficult. For numerical reasons, we sugest the following series expansion which is analytically equivalent to (12) but numerically better:

$$E_1(\boldsymbol{r}) = \sum_{p=0}^{P}\sum_{q=0}^{Q} \bar{a}_{pq}\cos^p(\phi)r^q + \sum_{p=1}^{P}\sum_{q=0}^{Q} \bar{b}_{pq}\sin(\phi)\cos^{p-1}(\phi)r^q \tag{13}$$

where the coefficients $\bar{a}_{pq}$ and $\bar{b}_{pq}$ are evaluated instead of a_{pq} and b_{pq}. $\bar{a}_{pq}, \bar{b}_{pq}$ are linearily related to a_{pq}, b_{pq}. Using the point-matching method, one can sample the equation at points (r_v, ϕ_u), $u = 0, 1, \ldots, 2P$; $v = 0, 1, \ldots, Q$, then the integral equation for the field $E_1(\boldsymbol{r})$ can be approximated by the matrix equation

$$\boldsymbol{Z}\boldsymbol{x} = \boldsymbol{y} \tag{14}$$

where

$$x_{(Q+1)p+q+1} = \begin{cases} \bar{a}_{pq}, & q = 0, \ldots, Q; \quad p = 0, \ldots, P \\ \bar{b}_{pq}, & q = 0, \ldots, Q; \quad p = P+1, \ldots, 2P \end{cases} \tag{15}$$

$$y_{(Q+1)u+v+1} = E_{i1}(r_v, \phi_u) \qquad (v = 0, \ldots, Q; \quad u = 0, \ldots, 2P) \tag{16}$$

$$Z_{(Q+1)u+v+1,(Q+1)p+q+1} = W_{(Q+1)p+q+1}(r_v, \phi_u) - \kappa \int_{\Omega_1} G_1^1(r_v, \phi_u, r', \phi') f(r', \phi') W_{(Q+1)p+q+1}(r', \phi') r' \, \mathrm{d}r' \, \mathrm{d}\phi' \tag{17}$$

with

$$W_{(Q+1)p+q+1}(r, \phi) = \begin{cases} \cos^p(\phi)r^q, & q = 0, \ldots, Q; \quad p = 0, \ldots, P \\ \sin(\phi) & \\ \times \cos^{p-1}(\phi)r^q, & q = 0, \ldots, Q; \quad p = P+1, \ldots, 2P. \end{cases} \tag{18}$$

Numerical integration of of the matrix $\boldsymbol{Z}$ can be carried out by Gaussian quadrature which is often faster than most other method [14]. Care must be taken in integrating over the singular point of the Green function. There are many ways to address singurality such as changing the integration variable, subtraction of singularity or simply ignoring the singularity if the contribution over an infinitestimal region around the singular point is negligible. The selection of P and Q can be done as follows. Starting with small values, P and Q are increased until the error between two consecutive solutions, i.e.,

$$\int_{\Omega_1} |E_{1,\text{current}}(\boldsymbol{r}, \bar{\boldsymbol{r}}) - E_{1,\text{previous}}(\boldsymbol{r}, \bar{\boldsymbol{r}})|^2 \, \mathrm{d}\Omega \tag{19}$$

is less than a predetermined value.

6. Reconstruction algorithm

6.1. Data collection setup

When the current source of magnitude I_0 is carried by a very long and thin solenoid, it is convenient to model it in terms of line sources

$$J(\boldsymbol{r}') = I_0\delta(\bar{\boldsymbol{r}} - \boldsymbol{r}') - I_0\delta(\bar{\boldsymbol{r}} - \boldsymbol{r}' - \Delta\boldsymbol{a}) \tag{20}$$

where $\bar{\boldsymbol{r}}$ and $\bar{\boldsymbol{r}} - \Delta\boldsymbol{a}$ are the positions of the two arms of the rectangular solenoid shown in figure 4. The current in each arm is modelled as a line source flowing in the opposite direction. The centre of the solenoid is at a distance r_3 from the centre of the pipe and the orientation

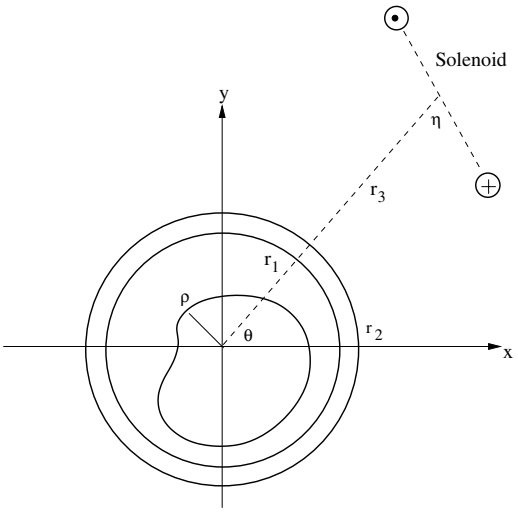

Figure 4. The position and orientation of the solenoid.

of the solenoid is described by angle η. The solenoid is rotated around the pipe to collect the scattered field which is used to reconstruct the extent of the solidification.

From (8) and (9), it follows that

$$E_1(\boldsymbol{r}, \bar{\boldsymbol{r}};\, f) = E_{i1}(\boldsymbol{r}, \bar{\boldsymbol{r}}) + \kappa \int_{\Omega_1} G_1^1(\boldsymbol{r}, \boldsymbol{r}') f(\boldsymbol{r}') E_1(\boldsymbol{r}', \bar{\boldsymbol{r}};\, f)\, \mathrm{d}\Omega' \tag{21}$$

$$E_3(\boldsymbol{r}, \bar{\boldsymbol{r}};\, f) = E_{i3}(\boldsymbol{r}, \bar{\boldsymbol{r}}) + \kappa \int_{\Omega_1} G_3^1(\boldsymbol{r}, \boldsymbol{r}') f(\boldsymbol{r}') E_1(\boldsymbol{r}', \bar{\boldsymbol{r}};\, f)\, \mathrm{d}\Omega' \tag{22}$$

where the incident field and scattered field, respectively, are

$$E_{iu}(\boldsymbol{r}, \bar{\boldsymbol{r}}) = -\mathrm{j}\omega\mu I_0 [G_u^3(\boldsymbol{r}, \bar{\boldsymbol{r}}) - G_u^3(\boldsymbol{r} - \Delta\boldsymbol{a}, \bar{\boldsymbol{r}})], \qquad u = 1, 3 \tag{23}$$

$$E_s(\boldsymbol{r}, \bar{\boldsymbol{r}};\, f) = \kappa \int_{\Omega_1} G_3^1(\boldsymbol{r}, \boldsymbol{r}') f(\boldsymbol{r}') E_1(\boldsymbol{r}', \bar{\boldsymbol{r}};\, f)\, \mathrm{d}\Omega'. \tag{24}$$

Once these equations for a particular line source configuration are solved, the fields due to an arbitrary solenoid shape can be obtained. Using (24), the voltage (and hence impedance) per unit length induced in the solenoid due to the scattered field can now be written as

$$V_s(\bar{\boldsymbol{r}};\, f) = E_s(\bar{\boldsymbol{r}}, \bar{\boldsymbol{r}};\, f) - E_s(\bar{\boldsymbol{r}} - \Delta\boldsymbol{a}, \bar{\boldsymbol{r}};\, f) = \kappa \int_{\Omega_1} H_3^1(\bar{\boldsymbol{r}}, \boldsymbol{r}') f(\boldsymbol{r}') E_1(\boldsymbol{r}', \bar{\boldsymbol{r}};\, f)\, \mathrm{d}\Omega' \tag{25}$$

where $H_3^1(\boldsymbol{r}, \boldsymbol{r}') = G_3^1(\boldsymbol{r}, \boldsymbol{r}') - G_3^1(\boldsymbol{r} - \Delta\boldsymbol{a}, \boldsymbol{r}')$. Since $V_s(\bar{\boldsymbol{r}};\, f)$ is a nonlinear functional of $f(\boldsymbol{r})$. Therefore, an iterative searching algorithm is necessary to retrieve $f(\boldsymbol{r})$ from $V_s(\bar{\boldsymbol{r}})$. At each iteration, the eddy-current distribution and the scattered field must be estimated based on the previous estimate of $f(\boldsymbol{r})$. A new estimate of $f(\boldsymbol{r})$ is then computed based on the error between the actual (measured) and the previous estimate of the scattered field.

6.2. First-order perturbation

Assume that we obtain an estimated profile f_b which is close to the function f. In the spirit of the Born approximation (BA) [16, 17], we can write

$$V_s(f;\, \bar{\boldsymbol{r}}) \approx \kappa \int_{\Omega_1} H_3^1(\bar{\boldsymbol{r}}, \boldsymbol{r}') f(\boldsymbol{r}') E_1(\boldsymbol{r}', \bar{\boldsymbol{r}};\, f_b)\, \mathrm{d}\Omega' \tag{26}$$

where $E_1(\boldsymbol{r}, \bar{\boldsymbol{r}}; f_b)$ is the electric field from equation (21) with the profile f_b. Equation (26) shows that the profile f is now linearly related to V_s. We now derive an iterative procedure to reconstruct the profile f within the Born approximation framework. However, it should be mentioned that Born approximation is not a necessary condition for the perturbation technique.

From (26), we define an error functional $U(f; \bar{\boldsymbol{r}})$:

$$U(f; \bar{\boldsymbol{r}}) = E_{s0}(\bar{\boldsymbol{r}}) - E_s(f; \bar{\boldsymbol{r}}) \tag{27}$$

where

$$E_{s0}(\bar{\boldsymbol{r}}) = \kappa \int_{\Omega_1} H_3^1(\bar{\boldsymbol{r}}, \boldsymbol{r}') f_0(\boldsymbol{r}') E_1(\boldsymbol{r}', \bar{\boldsymbol{r}}; f_0)\, \mathrm{d}\Omega' \tag{28}$$

and f_0 is the actual distribution that we want to reconstruct. $E_{s0}(\bar{\boldsymbol{r}})$ is the quantity that we can measure. Using (25) in (27) we can write the error functional as

$$U(f; \bar{\boldsymbol{r}}) = E_{s0}(\bar{\boldsymbol{r}}) - \kappa \int_{\Omega_1} H_3^1(\bar{\boldsymbol{r}}, \boldsymbol{r}') f(\boldsymbol{r}') E_1(\boldsymbol{r}', \bar{\boldsymbol{r}}; f)\, \mathrm{d}\Omega'. \tag{29}$$

If the measurements are taken at L different angles, we want to find such an f that minimizes $\sum_{l=1}^{L} |U(f; \bar{\boldsymbol{r}}_l)|^2$ subjected to the integral equation (21). We start with the first-order Taylor series expansion

$$|U(f + \delta f; \bar{\boldsymbol{r}})|^2 \approx |U(f; \bar{\boldsymbol{r}})|^2 + 2\mathrm{Re}\,[U^*(f; \bar{\boldsymbol{r}}) \delta U(f; \bar{\boldsymbol{r}})] \tag{30}$$

where $U^*(f; \bar{\boldsymbol{r}})$ is the conjugate of $U(f; \bar{\boldsymbol{r}})$, and $\delta U(f; \bar{\boldsymbol{r}})$ can be obtained using (29) with the spirit of the Born approximation (26):

$$\delta U(f; \bar{\boldsymbol{r}}) = -\kappa \int_{\Omega_1} H_3^1(\bar{\boldsymbol{r}}, \boldsymbol{r}') \delta f(\boldsymbol{r}') E_1(\boldsymbol{r}', \bar{\boldsymbol{r}}; f)\, \mathrm{d}\Omega'. \tag{31}$$

The variation in $f(\boldsymbol{r})$ is given by

$$\delta f(\boldsymbol{r}) = f_\alpha(\boldsymbol{r}) \delta\alpha + f_\rho(\boldsymbol{r}) \delta\rho(\phi) \tag{32}$$

where

$$f_\alpha(\boldsymbol{r}) = \frac{\partial f(\boldsymbol{r})}{\partial \alpha} = \frac{\rho(\phi) - r}{\pi[1 + \alpha^2[r - \rho(\phi)]^2]} \tag{33}$$

$$f_\rho(\boldsymbol{r}) = \frac{\partial f(\boldsymbol{r})}{\partial \rho} = \frac{\alpha}{\pi[1 + \alpha^2[r - \rho(\phi)]^2]}. \tag{34}$$

Note that as $\alpha \to \infty$ (there is no mushy zone), $f_\rho(\boldsymbol{r}) \to \delta[r - \rho(\phi)]$, $f_\alpha(\boldsymbol{r}) \to 0$. Under this condition, the double integrals in (31) are reduced to single integrals. The shape function $\rho(\phi)$ describes a simple closed curve with $0 \leqslant \phi \leqslant 2\pi$. For a smooth curve, it can be approximated by a truncated Fourier series of $2N + 1$ terms:

$$\rho(\phi) = \sum_{n=0}^{N} A(n) \cos(n\phi) + \sum_{n=1}^{N} B(n) \sin(n\phi) \tag{35}$$

where $A(n)$ and $B(n)$ are real coefficients to be determined. The perturbation in ρ is

$$\delta\rho(\phi) = \sum_{n=0}^{N} \delta A(n) \cos(n\phi) + \sum_{n=1}^{N} \delta B(n) \sin(n\phi). \tag{36}$$

An iterative procedure is used to update parameters $A(n)$, $B(n)$ and α until convergence. Equation (30) can now be written as

$$|U(f + \delta f; \bar{\boldsymbol{r}})|^2 \approx |U(f; \bar{\boldsymbol{r}})|^2 + \delta\alpha D(\bar{\boldsymbol{r}}) + \sum_{n=0}^{N} \delta A(n) C(n; \bar{\boldsymbol{r}}) + \sum_{n=1}^{N} \delta B(n) S(n; \bar{\boldsymbol{r}}) \tag{37}$$

where

$$C(n;\bar{\boldsymbol{r}}) = -2\mathrm{Re}\left[\kappa U^*(f;\bar{\boldsymbol{r}})\int_{\Omega_1} H_3^1(\bar{\boldsymbol{r}},\boldsymbol{r}')f_\rho(\boldsymbol{r}')\cos(n\phi')E_1(\boldsymbol{r}',\bar{\boldsymbol{r}};f)\,\mathrm{d}\Omega'\right] \tag{38}$$

$$S(n;\bar{\boldsymbol{r}}) = -2\mathrm{Re}\left[\kappa U^*(f;\bar{\boldsymbol{r}})\int_{\Omega_1} H_3^1(\bar{\boldsymbol{r}},\boldsymbol{r}')f_\rho(\boldsymbol{r}')\sin(n\phi')E_1(\boldsymbol{r}',\bar{\boldsymbol{r}};f)\,\mathrm{d}\Omega'\right] \tag{39}$$

$$D(n;\bar{\boldsymbol{r}}) = -2\mathrm{Re}\left[\kappa U^*(f;\bar{\boldsymbol{r}})\int_{\Omega_1} H_3^1(\bar{\boldsymbol{r}},\boldsymbol{r}')f_\alpha(\boldsymbol{r}')E_1(\boldsymbol{r}',\bar{\boldsymbol{r}};f)\,\mathrm{d}\Omega'\right]. \tag{40}$$

In matrix form, equation (37) can be expressed as

$$|U(\rho+\delta\rho;\bar{\boldsymbol{r}})|^2 \approx |U(\rho;\bar{\boldsymbol{r}})|^2 + \boldsymbol{p}^T(\bar{\boldsymbol{r}})\delta\boldsymbol{q} \tag{41}$$

where

$$\boldsymbol{p}(\bar{\boldsymbol{r}}) = \mathrm{vec}\{D(\bar{\boldsymbol{r}}), C(n;\bar{\boldsymbol{r}}), S(n;\bar{\boldsymbol{r}})\} \tag{42}$$

$$\boldsymbol{q} = \mathrm{vec}\{\alpha, A(n), B(n)\}. \tag{43}$$

For L measurements, (41) becomes

$$\boldsymbol{e} = \boldsymbol{u} + \boldsymbol{P}\delta\boldsymbol{q} \tag{44}$$

$$\boldsymbol{e} = \mathrm{vec}\{U(\bar{\boldsymbol{r}}_1; f+\delta f), \ldots, U(\bar{\boldsymbol{r}}_L; f+\delta f)\} \tag{45}$$

$$\boldsymbol{u} = \mathrm{vec}\{U(\bar{\boldsymbol{r}}_1; f), \ldots, U(\bar{\boldsymbol{r}}_L, f)\} \tag{46}$$

$$\boldsymbol{P} = \mathrm{vec}\{\boldsymbol{p}^T(\bar{\boldsymbol{r}}_1), \ldots, \boldsymbol{p}^T(\bar{\boldsymbol{r}}_L)\}L)\}. \tag{47}$$

Let $f_m(\boldsymbol{r})$ with the parameters $A_m(n)$, $B_m(n)$ and α_m, be the estimate of $f(\boldsymbol{r})$ after the mth iteration. The new estimate $f_{m+1} = f_m + \delta f_m$ can be found by such a δf_m that minimizes $\sum_{l=1}^{L}|U(f_m+\delta f_m;\boldsymbol{r}_l)|^2$. The best δf_m corresponding to $\delta\boldsymbol{q}_m$ is obtained by

$$\delta\boldsymbol{q}_m = \arg\min_{\boldsymbol{x}} \|\boldsymbol{u}_m + \boldsymbol{P}_m\boldsymbol{x}\|. \tag{48}$$

The solution to this problem is well known [18, ch 12, p 404].

7. Computational issues

To reconstruct the profile $f(\boldsymbol{r})$, we have to solve the forward part and the inverse part. Both of them require a lot of two-dimensional numerical intergration which is time consuming. Due to the complex geometry in our problem, the Green function is tedious and computationally demanding. In this section, we derive a procedure to speed up the computation considerably. The idea is based on the Gaussian quadrature formula [14]. The computation of the electric field in region Ω_1 by the moments method involves the computation of the matrix elements of $\boldsymbol{Z}$:

$$Z_{mn} = W_n(\boldsymbol{r}_m) - \int_0^{2\pi}\int_0^{r_1} G_1^1(\boldsymbol{r}_m,\boldsymbol{r}')f(\boldsymbol{r}')W_n(\boldsymbol{r}')r'\,\mathrm{d}r'\,\mathrm{d}\phi' \tag{49}$$

where $W_n(\boldsymbol{r}')$ is one of the basis functions defined in section 5. Dividing region Ω_1 into $K_1 \times K_2$ subregions, the double integral in (49) becomes

$$\int_0^{2\pi}\int_0^{r_1} G_1^1(\boldsymbol{r}_m,\boldsymbol{r}')f(\boldsymbol{r}')W_n(\boldsymbol{r}')r'\,\mathrm{d}r'\,\mathrm{d}\phi'$$

$$\approx \sum_{k_1=1}^{K_1}\sum_{k_2=1}^{K_2}\int_{\phi'_{k_1-1}}^{\phi'_{k_1}}\int_{r'_{k_2-1}}^{r'_{k_2}} G_1^1(\boldsymbol{r}_m,\boldsymbol{r}')f(\boldsymbol{r}')W_n(\boldsymbol{r}')r'\,\mathrm{d}r'\,\mathrm{d}\phi'. \tag{50}$$

Table 1. Values of the physical parameters.

Parameters	Notation	Value
Conductivity of solidified metal	σ_s	2×10^6 (mhos m^{-1})
Conductivity of molten metal	σ_l	1×10^6 (mhos m^{-1})
Conductivity of pipe	σ_p	1×10^5 (mhos m^{-1})
Inner radius of pipe	r_1	15×10^{-3} (m)
Outer radius of pipe	r_2	16×10^{-3} (m)
Radial distance of solenoid	r_3	30×10^{-3} (m)

In our iterative procedure, the profile changes after each iteration and hence the integral (49) has to be evaluated again and again. We will show that there is no need to do so. Using Gaussian quadrature, the matrix element Z_{mn} can now be written as

$$\begin{aligned} Z_{mn} \approx W_n(\boldsymbol{r}_m) - \sum_{k_1=1}^{K_1}\sum_{k_2=1}^{K_2} \frac{\phi'_{k_1}-\phi'_{k_1-1}}{2}\frac{r'_{k_2}-r'_{k_2-1}}{2} \sum_{i=1}^{N_1}\sum_{j=1}^{N_2} c_i d_j F_n \\ \times\left(\boldsymbol{r}_m, \frac{(r'_{k_2}-r'_{k_2-1})\rho_j + r'_{k_2}+r'_{k_2-1}}{2}, \frac{(\phi'_{k_1}-\phi'_{k_1-1})\varphi_i + \phi'_{k_1}+\phi'_{k_1-1}}{2}\right) \\ \times f\left(\frac{(r'_{k_2}-r'_{k_2-1})\rho_j + r'_{k_2}+r'_{k_2-1}}{2}, \frac{(\phi'_{k_1}-\phi'_{k_1-1})\varphi_i + \phi'_{k_1}+\phi'_{k_1-1}}{2}\right) \end{aligned} \tag{51}$$

where $F_n(\boldsymbol{r}, \boldsymbol{r}') = G_1^1(\boldsymbol{r}, \boldsymbol{r}')W_n(\boldsymbol{r}')r'$. The nodes ρ_j and φ_i are roots of the N_2th and N_1th degree Legendre polynomials respectively, and c_i, d_j are their associated weights. They are extensively tabulated in [15]. The function $F_n(\boldsymbol{r}_m, \boldsymbol{r}')$ can be pre-computed off-line except for the function $f(\boldsymbol{r})$ which is computationally very fast.

8. Simulation

Example 1. The physical parameters used in the simulation are listed in table 1.

To compute the elctric field inside the pipe, we need to select the number of basis functions, namely P and Q. In this simulation, we choose $P = 5$ and $Q = 5$; the direction of the solenoid is $\theta = \pi/2$ (refer to figure 4), and the frequency of excitation is 100 Hz. When the solidification layer is circular and there is no mushy zone, it is possible to find an analytical solution for the electric field. Figures 5 and 6 show the magnitude of the normalized electric field $E_1/(-\mathrm{j}\omega I_0)$ computed by the moments method, and the error compared with the analytical solution, respectively. It can be seen that the magnitude of the field is large when it is near the solenoid. The numerical solution is very accurate and the error is less than 0.03%.

Example 2. In the second simulation example, we use the same physical parameters as in the first one except the solidification is nonsymmetrical (figure 7) and the mushy zone is smooth ($\alpha = 3.0$). 15 measurements are taken and are shown in figure 8.

The eddy-current patterns inside the pipe are influenced by the geometry of the solidified metal layer, and the eddy currents are mostly flowing in this layer. This is because the conductivity of the solid metal is higher than that of the liquid metal. The second reason is associated with the skin effect whereas currents tend to flow in the outer surface of an object. The eddy-current distributions are shown in figures 9 and 10.

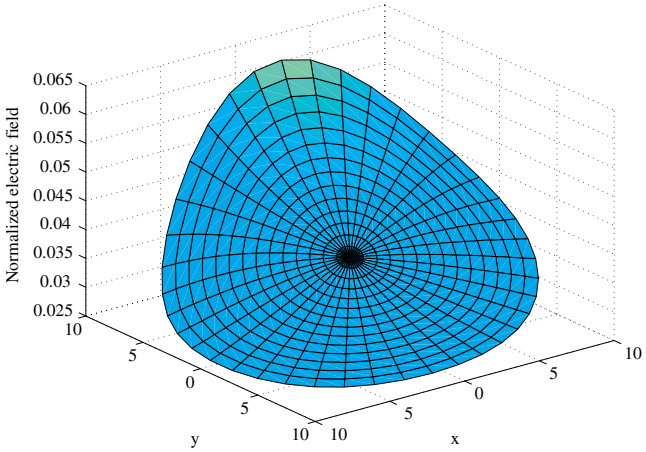

Figure 5. Magnitude of normalized electric field $\frac{E_1}{-j\omega I_0}$ for the circular domain.

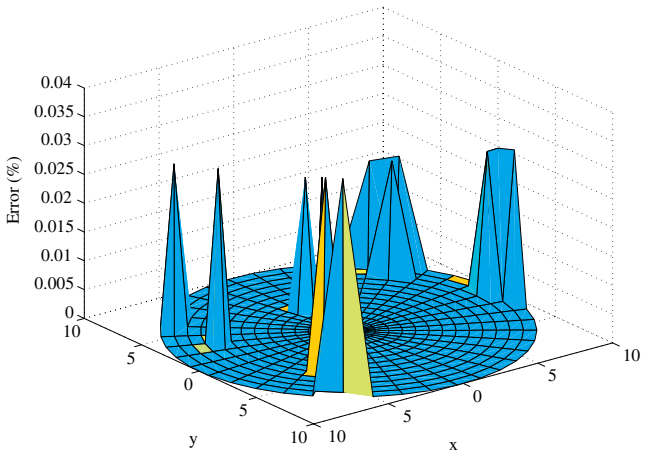

Figure 6. Error between numerical and analytical solutions of the electric field.

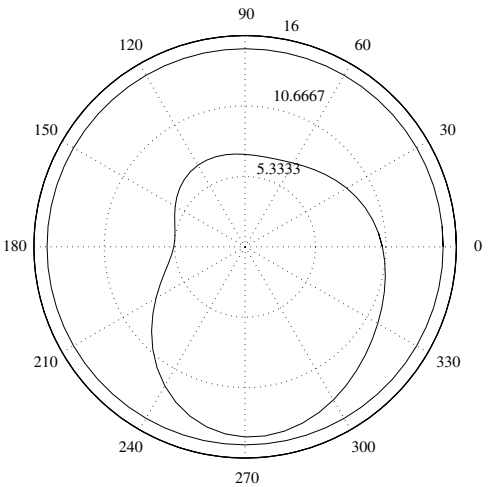

Figure 7. The geometry of solidification.

The initial estimate for ρ is assumed to be a circle. Since the solid–liquid boundary must occur within the pipe, the intial estimate of ρ must have a radius less than the inner radius of

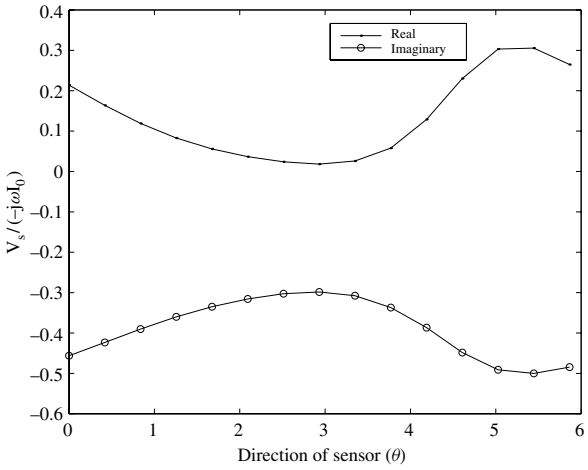

Figure 8. Normalized voltage versus the direction of the solenoid (θ).

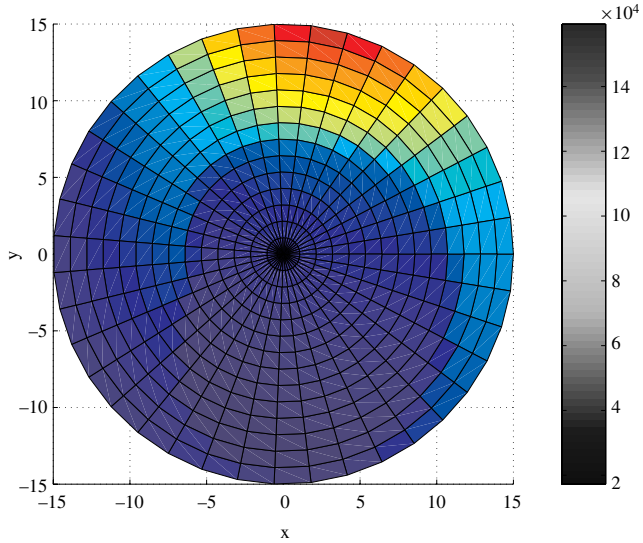

Figure 9. Real part of normalized eddy-current distribution.

the pipe. This constraint provides reasonable initial estimates for the iterative reconstruction procedure. Figure 11 depicts the estimates of the solid–liquid boundary after each of the first two iterations. Each iteration takes about 40 s CPU time. We define the relative mean square error (RMSE) of the conductivity distribution at the kth iteration as

$$\mathrm{RMSE}_\alpha = \sqrt{\frac{(\alpha_k - \alpha_0)^2}{\alpha_0^2}} \tag{52}$$

$$\mathrm{RMSE}_\rho = \sqrt{\frac{\sum_{n=0}^{N}(A_k - A_0)^2(n) + \sum_{n=1}^{N}(B_k - B_0)^2(n)}{\sum_{n=0}^{N} A_0^2(n) + \sum_{n=1}^{N} B_0^2(n)}} \tag{53}$$

where α_0, $A_0(n)$ and $B_0(n)$ are the actual parameters we want to estimate. It can be seen in figure 12 that the RMSE for $\rho(\phi)$ rapidly decreases after each successive iteration. The parameter α also converges quite well to the actual value. The effect of ρ is more dominant than that of α. This may be a reason why α tends to converge slower than ρ. The conductivity

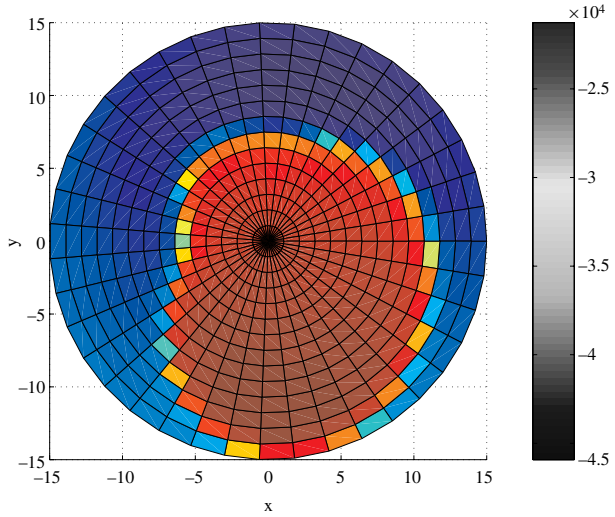

Figure 10. Imaginary part of normalized eddy-current distribution.

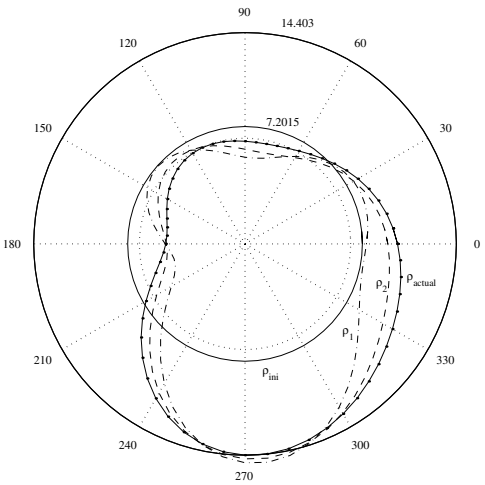

Figure 11. True shape and estimates after each of the first two iterations.

profile can now be reconstructed from the estimated parameters. We also observe that the reconstruction is quite unstable when η is close to 90° (refer to figure 4).

9. Conclusion

This paper has developed a theoretical framework for imaging the shape and thickness of metal solidification inside a pipe using a tranverse magnetic field. This work is believed to be the first of its kind in the area of metalurgical imaging. Using the superposition theorem and the Green functions, we derived a relationship between the conductivity distribution and the observable scattered field. Based on this relationship an iterative reconstruction algorithm was derived. At each iteration step, the electric field inside the pipe is solved numerically by the moments method with Fourier series and the polynomial approximation. The numerical results could be seen to be very accurate. The reconstruction algorithm established in this paper has been demonstrated to be fast convergent. The real data experimentation will be carried out soon and reported in the near future.

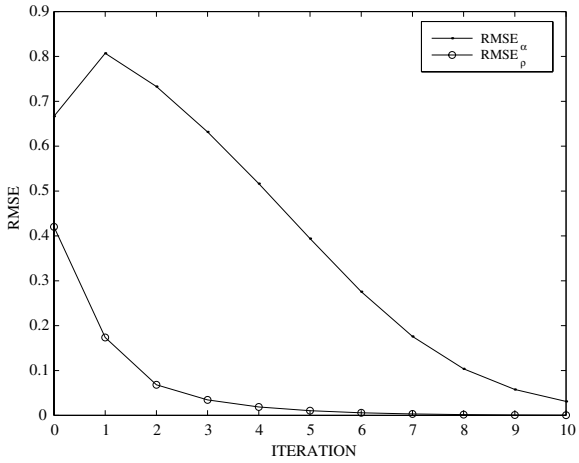

Figure 12. Relative error versus the number of iterations.

Acknowledgments

This work has been supported by the Australian Cooperative Research Centre for Sensor Signal and Information Processing (CSSIP) and the G K Williams Co-operative Research Centre for Extractive Metallurgy.

Appendix. Analytical form of the Green functions

The Green functions for cylindrically layered media can be constructed in terms of the infinite-space fields radiated by delta-function sources and the fields undergoing multiple reflections at boundaries [19]. The latter are solved from homogeneous differential equations. By matching the fields at the boundaries, the reflection and transmittion properties are uniquely determined. The infinite-space Green function is then incorporated to completely determine the Green functions.

The Green functions can be written as

$$G_1^1(\boldsymbol{r},\boldsymbol{r}') = \frac{1}{2\pi}K_0\left(k_1\sqrt{r^2+r'^2-2rr'\cos(\phi-\phi')}\right) + \frac{1}{2\pi}\sum_{m=0}^{\infty}\varepsilon_0^m\cos[m(\phi-\phi')]\frac{\alpha_{11}\beta_1+\alpha_{12}\beta_2}{\alpha_{21}\beta_1+\alpha_{22}\beta_2}I_m(kr)I_m(k_1r') \tag{54}$$

$$G_2^1(\boldsymbol{r},\boldsymbol{r}') = \frac{1}{2\pi}\sum_{m=0}^{\infty}\varepsilon_0^m\cos[m(\phi-\phi')] \times\frac{\beta_2}{\alpha_{21}\beta_1+\alpha_{22}\beta_2}I_m(k_1r')\left[K_m(k_2r)+I_m(k_2r)\frac{\beta_1}{\beta_2}\right] \tag{55}$$

$$G_3^1(\boldsymbol{r},\boldsymbol{r}') = \frac{1}{2\pi}\sum_{m=0}^{\infty}\varepsilon_0^m\cos[m(\phi-\phi')]\frac{1}{\alpha_{21}\beta_1+\alpha_{22}\beta_2}I_m(k_1r')K_m(k_3r) \tag{56}$$

where $\epsilon_0^m = 1$ if $m = 0$, 2 if $m \geqslant 1$ and†

$$\begin{aligned}
\alpha_{11} &= k_2 r_1 I'_m(k_2 r_1) K_m(k_1 r_1) - k_1 r_1 K'_m(k_1 r_1) I_m(k_2 r_1) \\
\alpha_{12} &= k_2 r_1 K'_m(k_2 r_1) K_m(k_1 r_1) - k_1 r_1 K'_m(k_1 r_1) K_m(k_2 r_1) \\
\alpha_{21} &= k_1 r_1 I'_m(k_1 r_1) I_m(k_2 r_1) - k_2 r_1 I'_m(k_2 r_1) I_m(k_1 r_1) \\
\alpha_{22} &= k_1 r_1 I'_m(k_1 r_1) K_m(k_2 r_1) - k_2 r_1 K'_m(k_2 r_1) I_m(k_1 r_1) \\
\beta_1 &= k_3 r_2 K'_m(k_3 r_2) K_m(k_2 r_2) - k_2 r_2 K'_m(k_2 r_2) K_m(k_3 r_2) \\
\beta_2 &= k_2 r_2 I'_m(k_2 r_2) K_m(k_3 r_2) - k_3 r_2 K'_m(k_3 r_2) I_m(k_2 r_2).
\end{aligned} \tag{57}$$

References

[1] Pitsillos J S, Yeow Y L and Gray N B 1997 Flow control in a subcooled tube: an experiment investigation of the effect of crust formation *Int. J. Heat Mass Transfer* **40** 4337–43

[2] Webster J G 1990 *Electrical Impedance Tomography* (Bristol: Adam Hilger)

[3] Sabbagh H A 1993 Materials evaluation *Am. Soc. Non-destruct. Test.* **53** 11

[4] McEleney P C 1992 Electromagnetic (Eddy current) testing *Nondestructive Testing Standards—Present and Future* (Philadelphia: ASTM STP) vol 1151, pp 63–70

[5] Wallace J P and Kunerth D C 1980 Eddy current response to metallic solidification in one dimension *Metall. Trans.* B **11** B 267–71

[6] Kunerth D C and Wallace J P 1980 Eddy current study of solidification in lead and lead 20 pct tin *Metall. Trans.* B **11** B 273–83

[7] Cook D P, Nishioka S and Evans J W 1995 A three-dimensional mathematical model of electromagnetic casting and testing against a physical model: II. Results from a physical model and testing of the mathematical model *Metall. Mater. Trans.* B **26** B 1271–9

[8] Crowley A B and Ockendon J R 1987 Modelling mushy regions *Appl. Sci. Res.* **44** 1–7

[9] Beckerman C, Bertram L A, Pien S J and Smelser R E 1992 *Micro/Macro Scale Phenomena in Solidification* HTD-vol 218/AMD-vol 139 (ASME)

[10] Stratton J A 1941 *Electromagnetic Theory* (New York: McGraw-Hill)

[11] Harrington R F 1967 Matrix methods for field problems *Proc. IEEE* **55** pp 136–49

[12] Harrington R F 1968 *Field Computation by Moments Method* (New York: Macmillan)

[13] Dudley D G 1985 Error minimization and convergence in numerical methods *Electromagnetics* **5** 89–97

[14] Atkinson K E 1988 *An Introduction to Numerical Analysis* (Singapore: Wiley)

[15] Abramowitz M and Stegun I A 1970 *Handbook of Mathematical Functions, with Formulae, Graphs, and Mathematical Tables* (New York: Dover)

[16] Devaney A J 1983 Inversion procedure for inverse scattering within the distorted-wave Born approximation *Phys. Rev. Lett.* **51** 237–40

[17] Chew W C and Liu Q H 1994 Inversion of induction tool measurements using the distorted Born iterative method and CG-FFHT *IEEE Trans. Geosci. Remote Sens.* **32** 878–84

[18] Golub G H and van Loan C F 1983 *Matrix Comput.* (Oxford: North Oxford Academic)

[19] Chew W C 1990 *Waves and Fields in Inhomogeneous Media* (New York: Van Nostrand-Reinhold)

† When $k_3 = 0$, we have to replace $K_m(k_3 r)$ by r^{-m} for all $m \geqslant 1$. $K_0(k_3 r)$ is replaced by $-\ln(r) + c$ where c is an unknown constant. This constant can be found if an additional condition is given (for example, the total current flowing through the cross section of conducting regions). In this paper, it is set to zero for simplicity.